Nanoscale

PAPER

View Article Online
View Journal | View Issue

Check for updates

Cite this: *Nanoscale*, 2017, **9**, 16680

A simple neridronate-based surface coating strategy for upconversion nanoparticles: highly colloidally stable ^{125}I-radiolabeled $NaYF_4$:Yb^{3+}/Er^{3+}@PEG nanoparticles for multimodal *in vivo* tissue imaging†

Uliana Kostiv,[a] Volodymyr Lobaz,[a] Jan Kučka,[a] Pavel Švec,[a] Ondřej Sedláček,[a] Martin Hrubý,[a] Olga Janoušková,[a] Pavla Francová,[b] Věra Kolářová,[b] Luděk Šefc[b] and Daniel Horák *[a]

Received 25th July 2017,
Accepted 1st October 2017

DOI: 10.1039/c7nr05456d

rsc.li/nanoscale

In this report, monodisperse upconversion $NaYF_4$:Yb^{3+}/Er^{3+} nanoparticles with superior optical properties were synthesized by the oleic acid-stabilized high-temperature co-precipitation of lanthanide chlorides in octadec-1-ene as a high-boiling organic solvent. To render the particles with biocompatibility and colloidal stability in bioanalytically relevant phosphate buffered saline (PBS), they were modified by using in-house synthesized poly(ethylene glycol)-neridronate (PEG-Ner), a bisphosphonate. The $NaYF_4$:Yb^{3+}/Er^{3+}@PEG nanoparticles showed excellent long-term stability in PBS and/or albumin without any aggregation or morphology transformation. The *in vitro* cytotoxicity of the nanoparticles was evaluated using primary fibroblasts (HF) and a cell line derived from human cervical carcinoma (HeLa). The particles were subsequently modified by using Bolton–Hunter-hydroxybisphosphonate to enable radiolabeling with ^{125}I for single-photon emission computed tomography/computed tomography (SPECT/CT) bimodal imaging to monitor the biodistribution of the nanoparticles in non-tumor mice. The bimodal upconversion ^{125}I-radiolabeled $NaYF_4$:Yb^{3+}/Er^{3+}@PEG nanoparticles are prospective for near-infrared (NIR) photothermal/photodynamic and SPECT/CT cancer theranostics.

Open Access Article. Published on 02 October 2017. Downloaded on 8/16/2024 3:05:35 PM.
This article is licensed under a Creative Commons Attribution 3.0 Unported Licence.

Introduction

Accurate imaging of contrast agents and therapeutics inside diseased cells deep within the body and the determination of their location are of crucial importance for the diagnosis of various diseases.[1,2] Radionuclide-based single-photon emission computed tomography (SPECT) on an anatomical background of computed tomography (CT) provides highly sensitive and quantitative molecular imaging. A complementary method, *in vivo* optical imaging, has the advantage of being a noninvasive and highly sensitive technique with no radiation burden and is widely used for the visualization of cellular and molecular functions in living organisms. Nevertheless, it has several limitations, especially the background autofluorescence of tissues and the lack of precise quantification because of its shallow visible light tissue penetration depth due to light scattering and absorbance by the tissues. As a result, more attention is paid to near infrared (NIR) optical imaging due to its ability to penetrate deeper through the tissue compared to conventionally used wavelengths in optical imaging.[3] Methods of molecular imaging suffer from relatively poor spatial resolution (1 mm) compared to anatomical imaging (CT and MRI; 0.1 mm and better). Using both SPECT/CT and NIR optical diagnostic modalities in a single experiment can give complementary information and compensate for the shortcomings of each imaging modality alone, resulting in an improved detection sensitivity and resolution for *in vitro*/*in vivo* tumor diagnosis and treatment.[4,5] Optical imaging is also a perfect tool for margin-free tumor resection in image-guided surgery.[6]

The emission of visible light under NIR irradiation is typically achieved by luminescent upconversion lanthanide (Ln) nanoparticles combining the energy of two NIR photons into

[a]*Institute of Macromolecular Chemistry, Academy of Sciences of the Czech Republic, Heyrovského nám. 2, 162 06 Prague 6, Czech Republic. E-mail: horak@imc.cas.cz*
[b]*Center for Advanced Preclinical Imaging, First Faculty of Medicine, Charles University, Salmovská 3, 120 00 Prague 2, Czech Republic*

†Electronic supplementary information (ESI) available: ^{31}P and ^{1}H NMR, 2D ^{1}H NMR COSY and MALDI-TOF spectra of synthesized compounds, details on BH-Ner synthesis and purification, radioactivity, intensity-weighted size distribution, autocorrelation decay plot, as well as hydrodynamic diameter of $NaYF_4$:Yb^{3+}/Er^{3+}@PEG and ^{125}I-labeled $NaYF_4$:Yb^{3+}/Er^{3+}@PEG nanoparticles. See DOI: 10.1039/c7nr05456d

This journal is © The Royal Society of Chemistry 2017

Open Access Article. Published on 02 October 2017. Downloaded on 8/16/2024 3:05:35 PM.
This article is licensed under a Creative Commons Attribution 3.0 Unported Licence.

one visible light photon.[7,8] This has attracted a great deal of interest due to its superior optical and magnetic properties[9] that can be easily controlled by varying the Ln ion dopants. Since the maximum particle absorption (980 nm) falls into the optical window in biological tissues, tissue penetration is relatively deep; those wavelengths are not absorbed by hemoproteins.[10] Other advantages of the particles include minimum autofluorescence, a large anti-Stokes shift, narrow emission bandwidths and low scattering, which strongly decreases with increasing wavelength ($\sim 1/\lambda^4$).[11] The upconversion nanoparticles composed of a $NaYF_4$ crystal host lattice and doped by an optically active Yb^{3+}/Er^{3+} ion pair are able after the sequential absorption of two or more low-energy NIR photons to convert them into high-energy visible emission, which may subsequently serve for efficient photodynamic or photothermal therapy *in situ*.[12,13] Upconversion nanoparticles are thus highly promising for various applications in biological fields, such as *in vitro* cell labelling,[14] *in vivo* multimodal imaging and cell tracking,[15] controlled drug delivery,[16] photodynamic therapy, photoacoustic therapy,[17] and photothermal therapy.[18,19] Chiefly, phototherapy generating singlet oxygen in cancer tissue is a very promising theranostic method for clinical oncology.[20]

Few articles have recently addressed potential $NaYF_4$:Yb^{3+}/Er^{3+} particle aggregation and dissolution in bioanalytically relevant media, such as phosphate buffered saline (PBS), and changes in the morphology, particle surface composition, Ln ion leakage, and photoluminescence intensity.[21,22] Though it is widely accepted that the $NaYF_4$:Yb^{3+}/Er^{3+}-based nanoparticles possess high photochemical and thermal stability and low solubility in water,[23] their properties can be strongly affected by certain anions and ligands present in the biological media.[22] In PBS, the $NaYF_4$:Yb^{3+}/Er^{3+} nanoparticles can undergo partial dissolution, subsequently forming stable Ln-phosphate complexes in the solution and on the particle surface due to the much lower solubility product of Ln-phosphates than that of the corresponding fluorides.[24] Moreover, this partial dissolution and particle morphological transformation under biological conditions may lead to organelle damage due to the stripping of the membrane phosphate groups from the lipid bilayer, which initiates pro-inflammatory effects and/or the generation of biological hazards in cells and animals.[25,26]

To prevent dissolution, preserve the luminescence, and reduce the possible toxicity of the $NaYF_4$:Yb^{3+}/Er^{3+} nanoparticles, a protective coating has to be introduced on the particle surface. In this respect, phosphonate moieties are considered the most effective anchoring agents to passivate the particle surface and prevent particle dissolution under biological conditions due to the high binding affinity of Ln ions to phosphate groups.[21,27–29] In combination with poly(ethylene glycol) (PEG), PEG-phosphonates can reduce the non-specific adsorption of proteins on the particles, prolong their blood circulation time, and prevent recognition by a reticuloendothelial system.[30] PEG-phosphonate-modified $NaYF_4$:Yb^{3+}/Er^{3+} nanoparticles carrying a single reactive group can provide a stable colloid in water, but they can aggregate in PBS.[31,32] In contrast, PEG-bisphosphonate ligands form a strong and stable link to Ln ions, providing long-term colloidal stability of the particles in both water and PBS.[9] However, the preparation of such ligands is quite laborious, requiring a multi-step synthesis.[33]

The aim of this work is to design high-quality, monodisperse, NIR-excitable upconversion $NaYF_4$:Yb^{3+}/Er^{3+} nanoparticles, modify their surface by PEG-hydroxybisphosphonate, in particular PEG-neridronate, *via* one-step ligand exchange, introduce functional groups for facile ^{125}I-radiolabeling and verify the colloidal stability of the particles in a physiological medium (PBS and/or albumin). The resulting ^{125}I-labeled $NaYF_4$:Yb^{3+}/Er^{3+}@PEG nanoparticles were tested in a non-tumor mouse model *via* SPECT/CT imaging. To the best of our knowledge, this is the first time that such highly colloidally stable biocompatible upconversion nanoparticles have been prepared. The nanoparticles were self-targeted into liver, which may be very valuable, *e.g.*, for NIR photothermal or photodynamic therapy (after the addition of a suitable photosensitizer) of liver tumors that are surgically very difficult to approach; at the same time, noninvasive imaging enables tracking of the fate of the nanoparticles over both short- and long-time periods.

Experimental

Chemicals and materials

Anhydrous yttrium(III), ytterbium(III) and erbium(III) chlorides (99%), ammonium hydrogen difluoride, octadec-1-ene (90%), phosphate buffered saline (PBS), 6-aminohexanoic acid, phosphorous acid, methanesulfonic acid, phosphorus trichloride, chloramine T hydrate (95%), L-ascorbic acid (99%), *N*,*N*′-dicyclohexylcarbodiimide (DCCI), 3-(4-hydroxyphenyl)propionic acid, and *N*-hydroxysuccinimide (NHS) were obtained from Sigma-Aldrich (St Louis, MO, USA). The PD-10 desalting column (Sephadex LH-20) was received from Amersham Biosciences, Sweden. Sephadex LH-20 was obtained from Sigma. Methoxy poly(ethylene glycol) succinimidyl active ester (PEG-NHS; M_w = 5000 g mol^{-1}) was purchased from Rapp Polymere (Tuebingen, Germany). Bovine serum albumin fraction V (BSA; M_w = 67 000 g mol^{-1}) was delivered by Serva Electrophoresis (Heidelberg, Germany). Oleic acid, methanol, hexane, dichloromethane, and propan-2-ol were obtained from Lach-Ner (Neratovice, Czech Republic). Na^{125}I radiolabeling solution (74 MBq) was purchased from the Institute of Isotopes (Budapest, Hungary). All of the other reagent grade chemicals were purchased from Sigma-Aldrich and used as received. A cellulose dialysis membrane (14 000 g mol^{-1}) was purchased from Spectrum Europe (Breda, Netherlands). Ultrapure Q-water ultra-filtered on a Milli-Q Gradient A10 system (Millipore; Molsheim, France) was used in all experiments.

Synthesis of $NaYF_4$:Yb^{3+}/Er^{3+} nanoparticles

$NaYF_4$:Yb^{3+}/Er^{3+} nanoparticles were synthesized according to a reported procedure.[34] Briefly, YCl_3 (0.78 mmol), $YbCl_3$

Open Access Article. Published on 02 October 2017. Downloaded on 8/16/2024 3:05:35 PM.
This article is licensed under a Creative Commons Attribution 3.0 Unported Licence.

(0.2 mmol), $ErCl_3$ (0.02 mmol), oleic acid (6 ml), and octadec-1-ene (15 ml) were charged in a 100 ml three-neck flask. The mixture was heated to 160 °C for 30 min with stirring under an argon atmosphere to obtain a homogeneous solution, which was cooled to room temperature (RT). NaOH (4 mmol) and $NH_4F{\cdot}HF$ (2.5 mmol) were dissolved in methanol (10 ml), and the solution was added dropwise to the above mixture, which was slowly heated at 70 °C under an argon atmosphere until methanol evaporation at 300 °C for 1.5 h. After cooling to RT, the $NaYF_4$:Yb^{3+}/Er^{3+} particles were precipitated with acetone (10 ml), collected by centrifugation (6000 rpm, 10 min), and washed with ethanol, 0.01 M HCl (10 ml), and water. Finally, the particle dispersion was dialyzed against water for 48 h.

Synthesis of sodium neridronate

Sodium neridronate, (6-amino-1-hydroxy-1-phosphono-hexyl) phosphonic acid monosodium salt, was prepared according to a previously published report with a slight modification.[35] Typically, 6-aminohexanoic acid (25 g; 190.6 mmol), phosphorous acid (15.63 g; 190.6 mmol), and methanesulfonic acid (80 ml) were placed into a flask equipped with a reflux condenser and a $CaCl_2$ tube and heated to 65 °C. Phosphorus trichloride (35 ml; 401.2 mmol) was added dropwise, and the mixture was maintained at 70 °C for 18 h, cooled to RT, and quenched into an ice-water mixture (200 ml) with vigorous stirring, and the resulting solution was refluxed for 5 h. After cooling to RT, the pH was adjusted to 4.4 with 50% aqueous solution of NaOH, and the formed suspension was aged at 0 °C for 2 h. The resulting neridronate was collected by filtration, washed with cold water (2 × 50 ml) and 95% ethanol (100 ml), and vacuum-dried as a white solid (29.19 g; 55%). ^{1}H NMR (300 MHz, D_2O) δ 3.00 (t, J = 7.4 Hz, 2H), 2.03–1.83 (m, 2H), 1.77–1.53 (m, 4H), 1.48–1.33 (m, 2H). ^{31}P NMR (121.5 MHz, D_2O) δ 19.65.

Synthesis of PEG-neridronate (PEG-Ner)

A solution of sodium neridronate (0.64 g, 2 mmol) in PBS (pH 7.4) was cooled to 5 °C; dry MeO-PEG-NHS (M_w = 5000 g mol^{-1}; 1 g; 0.2 mmol of NHS groups) was added, the mixture was stirred at 5 °C for 5 h, and the product was separated on a Sephadex G25 column with a water eluent and freeze-dried. ^{1}H NMR (600 MHz, D_2O, δ): 3.68 (s, –O–CH_2–CH_2–O–, 4H), 3.37 (s, –CH_3, 3H), 3.21–3.17 (t, CH_2, 2H), 2.50 (s, CO–CH_2–CH_2–CO, 4H), 1.99–1.92 (t, CH_2, 2H), 1.59–1.55 (t, CH_2, 2H) 1.53–1.50 (t, CH_2, 2H) 1.33–1.30 (t, CH_2, 2H); ^{13}C NMR (150.9 MHz, D_2O, δ): 177.9, 177.4, 77.0, 73.6, 72.2, 60.7, 42.0, 41.6, 33.8, 30.7, 29.6, 25.9 ppm; ^{31}P NMR (121.5 MHz, D_2O, δ): 19.69 ppm (Fig. S1 in the ESI†). The substitution of NHS end-groups of PEG with neridronate calculated from ^{1}H NMR was 54%.

Synthesis of Bolton–Hunter reagent

Bolton–Hunter reagent (*N*-succinimidyl-3-(4-hydroxyphenyl) propionate) (BH) was prepared according to the previously described procedure.[36] Briefly, a solution of DCCI (3 g; 14.6 mmol) in dichloromethane (5 ml) was added dropwise to an ice-cold mixture of 3-(4-hydroxyphenyl)propionic acid (2.17 g; 13.1 mmol) and NHS (1.68 g; 14.6 mmol) in dichloromethane (20 ml). After stirring at 4 °C for 5 h, the white precipitate was filtered off, and the solution was evaporated under vacuum. The crude product was recrystallized from propan-2-ol to afford the BH as white crystals (2.06 g, 60%). ^{1}H NMR (300 MHz, $CDCl_3$) δ ppm 7.07 (d, 2H), 6.76 (d, 2H), 2.98 (t, 2H) 2.86 (t, 2H), 2.82 (s, 4H). Mass spectroscopy (MS) ESI^+: m/z 263.14 $[M]^+$. Elemental analysis calculated for $C_{13}H_{13}NO_5$: C, 59.31; H, 4.98; N, 5.32. Found: C, 59.45; H 5.02; N, 5.28.

Synthesis of Bolton–Hunter-neridronate (BH-Ner)

The solution of sodium neridronate (0.138 g; 0.43 mmol) in PBS (pH 7.4) was cooled to 5 °C, dry Bolton–Hunter reagent (0.103 g; 0.39 mmol) was added, and the mixture was stirred at 5 °C for 5 h. The product denoted as Bolton–Hunter-neridronate (BH-Ner) was isolated by precipitation with propan-2-ol and vacuum-dried. ^{1}H NMR (600 MHz, D_2O, δ): 7.07 (d, 2H; Ar), 6.83 (d, 2H; Ar), 2.99 (t, 2H; CH_2), 2.80 (t, 2H; CH_2), 2.44 (t, 2H; CH_2), 1.91 (m, 2H; CH_2), 1.39 (m, 2H; CH_2), 1.26 (m, 2H; CH_2), and 0.95 (m, 2H; CH_2). Additional characterization of BH-Ner with 2D ^{1}H NMR COSY spectroscopy, details of the synthesis and purification are available in the ESI (Fig. S2–S5†). MS (MALDI-TOF): m/z 426.19 $[M\ H]^+$ (Fig. S6 in ESI†). Yield: 62.5 mol% of sodium neridronate substituted with Bolton–Hunter reagent.

Synthesis of $NaYF_4$:Yb^{3+}/Er^{3+}@PEG and $NaYF_4$:Yb^{3+}/Er^{3+}@PEG-BH-Ner nanoparticles

PEG-Ner (12 mg) was added to the aqueous dispersion of $NaYF_4$:Yb^{3+}/Er^{3+} nanoparticles (3 ml; 6 mg ml^{-1}) at RT with stirring for 24 h under formation of $NaYF_4$:Yb^{3+}/Er^{3+}@PEG nanoparticles. Subsequently, BH-Ner (1 mg) was added and stirring continued for an additional 24 h. $NaYF_4$:Yb^{3+}/Er^{3+}@PEG and $NaYF_4$:Yb^{3+}/Er^{3+}@PEG-BH-Ner nanoparticles were dialyzed against water and filtered through a Millex-HA syringe filter unit, 0.45 μl pore size, until reaching a concentration of 6 mg ml^{-1}.

Synthesis of ^{125}I-radiolabeled $NaYF_4$:Yb^{3+}/Er^{3+}@PEG nanoparticles

$NaYF_4$:Yb^{3+}/Er^{3+}@PEG-BH-Ner nanoparticles were labeled with radioiodine by the chloramine T method with minor modifications.[37] Briefly, $NaYF_4$:Yb^{3+}/Er^{3+}@PEG-BH-Ner nanoparticles (1 mg), chloramine T (15 μl; 10 mg ml^{-1} of PBS), and $Na^{125}I$ radiolabeling solution (25 μl; 150 MBq) were dissolved in PBS buffer (300 μl; pH 7.4) and incubated at RT for 3 h with continuous shaking. A solution of ascorbic acid (25 mg ml^{-1} PBS) was added, and the reaction continued for 20 h. The resulting ^{125}I-labeled $NaYF_4$:Yb^{3+}/Er^{3+}@PEG nanoparticles were passed through the PD-10 desalting column with PBS as the mobile phase to remove the residual ^{125}I and low-molecular-weight residues; altogether, 20 fractions (0.75 ml each) were collected. Radioactivity of the nanoparticle solutions was measured using a Bqmetr 4 ionization chamber (Empos; Prague, Czech Republic). The labeling yield was calculated as the activity of the ^{125}I-labeled $NaYF_4$:Yb^{3+}/Er^{3+}@PEG nanoparticles relative to

 This journal is © The Royal Society of Chemistry 2017

Open Access Article. Published on 02 October 2017. Downloaded on 8/16/2024 3:05:35 PM.
This article is licensed under a Creative Commons Attribution 3.0 Unported Licence.

the total activity of the starting mixture. The concentration of particles was 6 mg ml^{-1}.

Characterization of the nanoparticles

The morphology of the nanoparticles was investigated by using a Tecnai G2 Spirit Twin 12 transmission electron microscope (TEM; FEI; Brno, Czech Republic). The size and nanoparticle size distribution were determined by measuring at least 500 nanoparticles from six random TEM micrographs using Atlas software (Tescan, Brno, Czech Republic). The number-average diameter (D_n), weight-average diameter (D_w) and the uniformity (polydispersity index PDI) were calculated as follows:

$$D_n = \sum N_i D_i / \sum N_i, \quad (1)$$

$$D_w = \sum N_i {D_i}^4 / \sum N_i {D_i}^3, \quad (2)$$

$$PDI = D_w / D_n, \quad (3)$$

where N_i and D_i are the number and diameter of the particle, respectively.

The hydrodynamic nanoparticle diameter (D_h), size distribution (polydispersity PD), and ζ-potential were determined by dynamic light scattering (DLS) on a ZEN 3600 Zetasizer Nano Instrument (Malvern Instruments; Malvern, UK). The particle dispersion was measured at 25 °C, and the D_h and PD were calculated from the intensity-weighted distribution function obtained by CONTIN analysis of the correlation function embedded in Malvern software.

Thermogravimetric analysis (TGA) was performed in nitrogen using a PerkinElmer TGA 7 analyzer (Norwalk, CT, USA) from 30 to 850 °C at a heating rate of 10 °C min^{-1}.

The cytotoxicity of the nanoparticles was evaluated using a primary fibroblast cell line (HF) and a cervical carcinoma cell line HeLa. 5×10^4 of HeLa or 8×10^4 of HF cells were seeded in 100 μl of media into 96-well flat-bottom TPP® plates (Sigma-Aldrich) for 24 h before adding the nanoparticles, the concentration of which varied in the range 0.5–600 μg ml^{-1}. The cells were cultivated at 37 °C for 72 h under a 5% CO_2 atmosphere. AlamarBlue® cell viability reagent (10 μl; Thermo Scientific) was added to each well and incubated at 37 °C for 4 h. The active component of the AlamarBlue® reagent resazurin was reduced to the highly fluorescent resorufin only in viable cells. Its fluorescence was detected in a Synergy Neo plate reader (Bio-Tek; Winooski, VT, USA) using an excitation at 570 nm and an emission at 600 nm. As a control, the cells cultivated in medium without nanoparticles were employed. Three wells were used for each concentration. The assay was repeated two times in triplicate.

Experimental animals

Two 12-weeks-old female adult BALB/C mice (Charles River; Cologne, Germany) were bred in the institutional animal specific-pathogen free facility and maintained in individually ventilated cages (12 : 12 h light–dark cycle, 22 ± 1 °C, 60 ± 5% humidity). The experiments were performed in accordance with national and international guidelines for laboratory animal care and approved by the Laboratory Animal Care and Use Committee of the First Faculty of Medicine, Charles University in Prague and the Ministry of Education, Youth and Sports and of the Czech Republic (MSMT-6316/2014-46).

SPECT/CT biodistribution experiment

^{125}I-labeled $NaYF_4:Yb^{3+}/Er^{3+}$@PEG nanoparticle dispersion in PBS buffer (100 μl) was injected intravenously *via* the tail vein into two mice (activity 30 MBq per mouse). The biodistribution was studied under anesthesia with 2% isoflurane in air using an Albira SPECT/PET/CT tri-modal preclinical scanner (Albira Imaging System, Bruker BioSpin; Rheinstetten, Germany). Both mice were screened at 30 min, 90 min, 24 h, and 96 h post-injection. All acquisitions used a set of multi-pinhole collimators. The duration of acquisition was 20 min (40 s per projection) followed by a single CT scan (8 min). Image analysis and co-registration were carried out using PMOD analysis software (PMOD Technologies LLC; Zürich, Switzerland).

Results and discussion

Highly colloidally stable upconversion particles in PBS: modification of $NaYF_4:Yb^{3+}/Er^{3+}$ with PEG-Ner

Upconversion $NaYF_4:Yb^{3+}/Er^{3+}$ nanoparticles of superior quality were synthesized by the high-temperature co-precipitation of lanthanide chlorides in a high-boiling solvent (octadec-1-ene) at 300 °C; oleic acid served as a stabilizer. The chemical composition and crystal structure of the particles were described earlier.[34] Oleic acid-stabilized $NaYF_4:Yb^{3+}/Er^{3+}$ nanoparticles had a spherical shape with D_n = 26 nm and a narrow size distribution (PDI = 1.01; Fig. 1a). The $NaYF_4:Yb^{3+}/Er^{3+}$ particles were hydrophobic due to the presence of the oleic acid capping ligand. Such particles cannot be dispersed in aqueous media, as required in biological systems. To obtain water-dispersible particles, the $NaYF_4:Yb^{3+}/Er^{3+}$ nanoparticles were treated with HCl, which removed oleic acid from the particle surface.[38] No changes in the particle size (D_n = 26), morphology, and size distribution (PDI = 1.02) were detected after the HCl treatment (Fig. 1b).

The oleic acid-free (naked) $NaYF_4:Yb^{3+}/Er^{3+}$ nanoparticles aggregated in water, reaching a hydrodynamic diameter of 360 nm (PD = 0.36), although they possessed a high positive surface charge (ζ-potential = 48 mV). For prospective biomedical applications, the particles should not be dispersible only in water, but they should also form stable and nontoxic colloids in physiological fluids (PBS). However, the naked $NaYF_4:Yb^{3+}/Er^{3+}$ nanoparticles quickly aggregated in PBS, forming a turbid dispersion most plausibly due to surface phosphate chelation and increased ionic strength in PBS compared to water, which compromised the electrostatic colloid stabilization.

To transfer the naked $NaYF_4:Yb^{3+}/Er^{3+}$ particles into PBS and prevent their aggregation, post-synthesis particle coating was used, ensuring steric stabilization consisting of an

Open Access Article. Published on 02 October 2017. Downloaded on 8/16/2024 3:05:35 PM.
This article is licensed under a Creative Commons Attribution 3.0 Unported Licence.

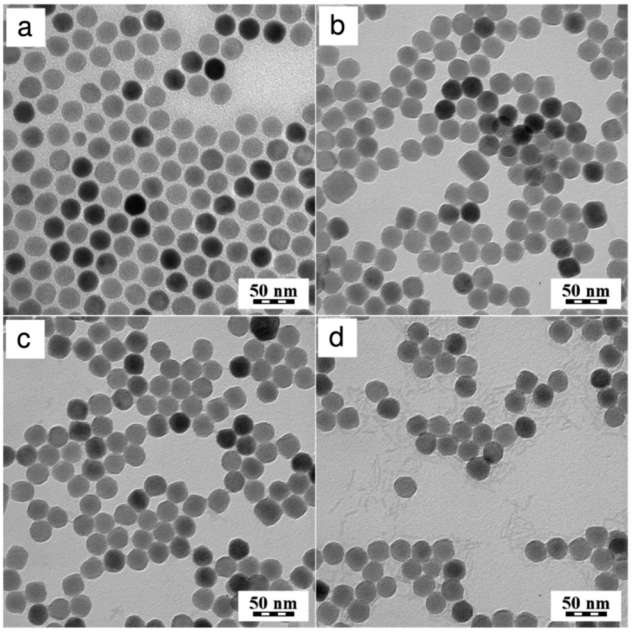

Fig. 1 TEM micrographs of (a) oleic acid-stabilized $NaYF_4$:Yb^{3+}/Er^{3+} nanoparticles in hexane, (b) naked $NaYF_4$:Yb^{3+}/Er^{3+} nanoparticles in water, and $NaYF_4$:Yb^{3+}/Er^{3+}@PEG in (c) water and (d) PBS after 3 months of storage.

addition of an in-house synthesized PEG-Ner (Fig. S7 in ESI†). Hydroxybisphosphonates have an advantage in that they possess a very strong affinity to lanthanide cations, which stabilizes the particles even in aqueous solutions of high ionic strength such as PBS.[21,39] PEG is attached to the nanoparticles *via* a coordination bond (chelate) formed between PEG-Ner and lanthanide cations on the particle surface. Shapes and sizes of the resulting $NaYF_4$:Yb^{3+}/Er^{3+}@PEG nanoparticles in water were observed using TEM (Fig. 1c). Due to the low electron density of polymers, the PEG layer was not noticeable in the TEM micrograph of the particles. The particles were individual without noticeable aggregation and had a regular spheroid shape with a number-average diameter D_n = 26 nm and a polydispersity index PDI = 1.02, documenting a very narrow particle size distribution. Such a narrow particle size distribution is highly necessary in bioapplications to achieve uniform bioavailability and stability of the particles once they are administered to the living organism.

To confirm the TEM results, the $NaYF_4$:Yb^{3+}/Er^{3+}@PEG particles dispersed in PBS buffer and/or BSA were investigated by DLS. The hydrodynamic diameter D_h and polydispersity PD of the nanoparticles in PBS were approximately 110 nm and 0.22, respectively. These values are larger than the D_n according to TEM, due to the effect of the polymer coating. It is worth mentioning that while DLS was measured in PBS, TEM analyzed the dry particle size. Moreover, intensity-weighted distributions measured by DLS provide the *Z*-average particle size, which is substantially larger than D_n. To exclude the effect of the potential dissolution of the $NaYF_4$:Yb^{3+}/Er^{3+}@PEG nanoparticles in PBS, they were aged in PBS for 3 months. No visible changes in the particle morphology, shape, or colloidal stability were detected by either TEM (Fig. 1d) or DLS (D_h = 120 nm, PD = 0.23). Moreover, to mimic blood conditions, the colloidal stability of the $NaYF_4$:Yb^{3+}/Er^{3+}@PEG particles was investigated in PBS in the presence of BSA (0.5 mg ml^{-1}), confirming that this protein did not change either the D_h or PD of the particles (Fig. 2a and Fig. S8 in ESI†).

To confirm the surface modification of the particles, the ζ-potential of the $NaYF_4$:Yb^{3+}/Er^{3+}@PEG nanoparticles was

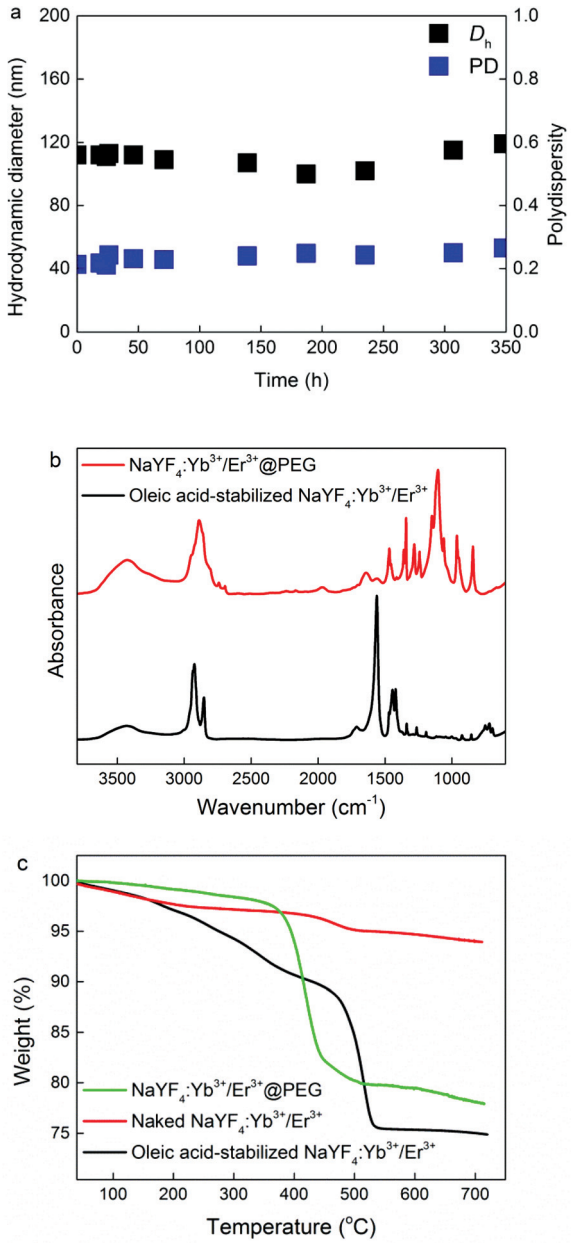

Fig. 2 (a) Hydrodynamic diameter D_h and polydispersity PD of $NaYF_4$:Yb^{3+}/Er^{3+}@PEG nanoparticles in PBS in the presence of BSA (0.5 mg ml^{-1}). (b) ATR FTIR spectra of oleic acid-stabilized $NaYF_4$:Yb^{3+}/Er^{3+} and $NaYF_4$:Yb^{3+}/Er^{3+}@PEG nanoparticles. (c) TGA of oleic acid-stabilized $NaYF_4$:Yb^{3+}/Er^{3+}, naked $NaYF_4$:Yb^{3+}/Er^{3+}, and $NaYF_4$:Yb^{3+}/Er^{3+}@PEG nanoparticles.

This journal is © The Royal Society of Chemistry 2017

Open Access Article. Published on 02 October 2017. Downloaded on 8/16/2024 3:05:35 PM.
This article is licensed under a Creative Commons Attribution 3.0 Unported Licence.

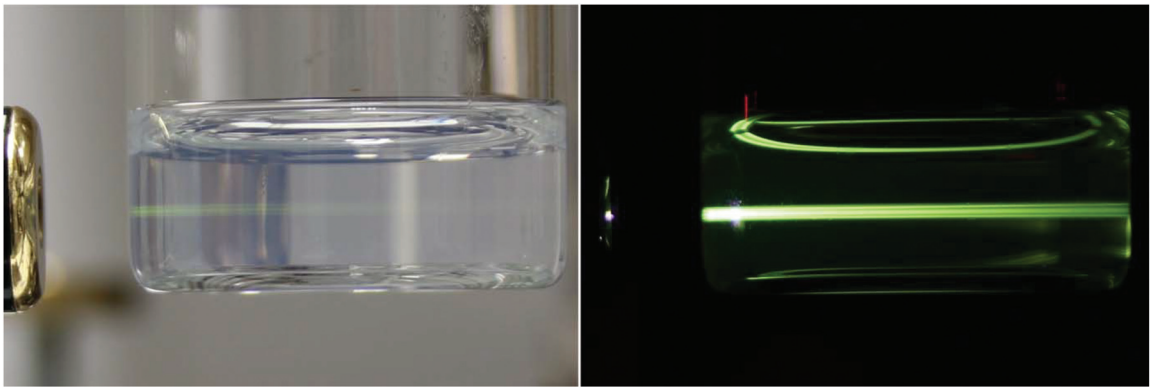

Fig. 3 Upconversion photoluminescent images of $NaYF_4:Yb^{3+}/Er^{3+}$@PEG nanoparticles in water (4 mg ml^{-1}) after excitation by a 980 nm laser with a power of 400 mW.

measured in water (pH 7). The particles showed a low positive charge (8 mV), which was significantly different from that of the initial measurement of naked $NaYF_4:Yb^{3+}/Er^{3+}$ nanoparticles (48 mV). Therefore, the ζ-potential measurements allowed us to conclude that the particles were sterically stabilized by PEG-Ner and uncharged PEG chains attached to the particles surface brought the particle slipping plane upwards from the charged surface, resulting in a near-neutral ζ-potential value.

The surfaces of oleic acid-stabilized $NaYF_4:Yb^{3+}/Er^{3+}$ and $NaYF_4:Yb^{3+}/Er^{3+}$@PEG nanoparticles were further verified by ATR FTIR spectroscopy (Fig. 2b). The spectrum of the initial oleic acid-stabilized $NaYF_4:Yb^{3+}/Er^{3+}$ nanoparticles exhibited characteristic asymmetric and symmetric C–H stretching vibrations (2924 and 2853 cm^{-1}, respectively) and COO^- vibrations (1562 and 1443 cm^{-1}) of oleic acid.[40] After surface modification by PEG-Ner, the characteristic oleic acid vibrations in the spectrum of $NaYF_4:Yb^{3+}/Er^{3+}$@PEG nanoparticles completely vanished. New intensive peaks appeared at 2887 and 1342 cm^{-1} corresponding to C–H stretching and bending vibrations, respectively; a strong peak at 1104 cm^{-1} was attributed to C–O stretching vibrations, and a broad peak at 3420 cm^{-1} corresponded to OH stretching vibrations.[41,42] The absence of oleic acid vibrations and the presence of the new PEG-Ner bands proved the successful surface modification of the $NaYF_4:Yb^{3+}/Er^{3+}$@PEG particles by ATR FTIR spectroscopy.

Additional analysis of the particle surface modification involved TGA (Fig. 2c). Small weight losses from RT to approximately 150 °C were ascribed to the evaporation of residual solvents, such as water or hexane. In the thermogram of oleic acid-stabilized $NaYF_4:Yb^{3+}/Er^{3+}$ nanoparticles, a major weight loss (~23 wt%) was detected at 200–500 °C due to oleic acid decomposition. In contrast, weight loss in the thermogram of the naked $NaYF_4:Yb^{3+}/Er^{3+}$ particles was rather low (~3 wt%), confirming the almost complete removal of oleic acid from the particle surface during treatment with HCl. Finally, main weight loss (~20 wt%) during TGA was attributed to decomposition of PEG-Ner on the $NaYF_4:Yb^{3+}/Er^{3+}$@PEG nanoparticle surface confirming efficiency of the coating.

The upconversion $NaYF_4$ nanoparticles doped by optically active Yb^{3+}/Er^{3+} ion pairs emit green and red light after NIR excitation. The green emissions of optically transparent $NaYF_4:Yb^{3+}/Er^{3+}$@PEG particle dispersions in water upon 980 nm excitation are shown in Fig. 3. A full description of upconversion photoluminescence spectra of the oleic acid-stabilized $NaYF_4:Yb^{3+}/Er^{3+}$ nanoparticles was presented in our previous report.[34]

Radiolabeling of $NaYF_4:Yb^{3+}/Er^{3+}$@PEG nanoparticles

Due to the lack of functional groups on the $NaYF_4:Yb^{3+}/Er^{3+}$@PEG nanoparticles, which are needed for subsequent radiolabeling, for the first time BH-Ner was selected as a tyrosine-containing reagent that can be easily labeled with radioiodine. The BH-Ner also contains bisphophonate moieties, which strongly anchor to the particle surface. The BH-Ner was obtained by the conjugation of neridronate with the Bolton–Hunter reagent *via* NHS-activated carboxy groups. BH-Ner was then bound to the $NaYF_4:Yb^{3+}/Er^{3+}$@PEG nanoparticles between the PEG chains attached on the inorganic core surface to yield $NaYF_4:Yb^{3+}/Er^{3+}$@PEG-BH-Ner particles. Subsequently, the particles were labeled with $Na^{125}I$ by the conventional chloramine T method to follow their fate in the organism by noninvasive PET/SPECT imaging. The reaction between ^{125}I and $NaYF_4:Yb^{3+}/Er^{3+}$@PEG-BH-Ner nanoparticles was monitored by measuring radioactivity in an ionization chamber (Fig. S9 in the ESI†). High radiolabeling yield (75%, *i.e.*, fraction 5–7) confirmed successful conjugation of ^{125}I to $NaYF_4:Yb^{3+}/Er^{3+}$@PEG-BH-Ner particles. As a control, $NaYF_4:Yb^{3+}/Er^{3+}$@PEG particles (without BH-Ner) were labeled with $Na^{125}I$; radiolabeling yield was rather low (~15%) probably due to non-specific radioiodine adsorption. The long-term colloidal stability of the ^{125}I-labeled $NaYF_4:Yb^{3+}/Er^{3+}$@PEG nanoparticles in PBS in the presence of ascorbic acid was supported by DLS studies. The hydrodynamic diameter of ^{125}I-labeled $NaYF_4:Yb^{3+}/Er^{3+}$@PEG nanoparticles did not change with time

Open Access Article. Published on 02 October 2017. Downloaded on 8/16/2024 3:05:35 PM.
This article is licensed under a Creative Commons Attribution 3.0 Unported Licence.

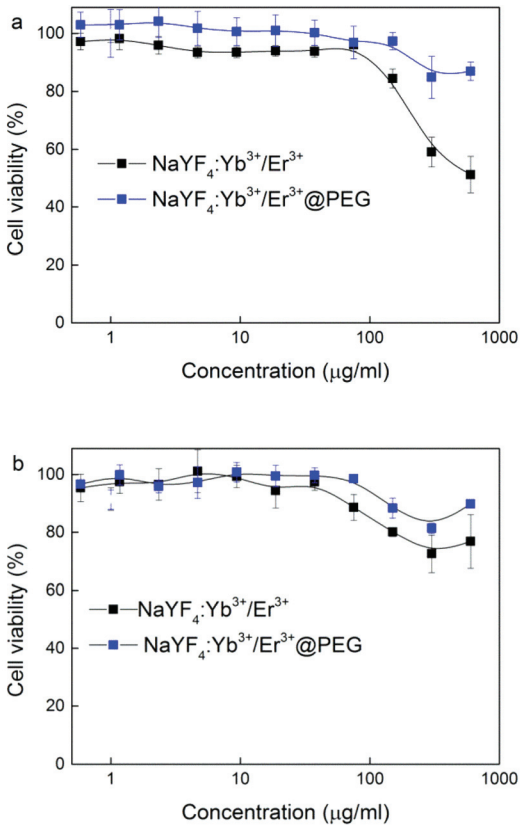

Fig. 4 Dependence of (a) HF and (b) HeLa cell viability on $NaYF_4:Yb^{3+}/Er^{3+}$ and $NaYF_4:Yb^{3+}/Er^{3+}$@PEG nanoparticle concentration.

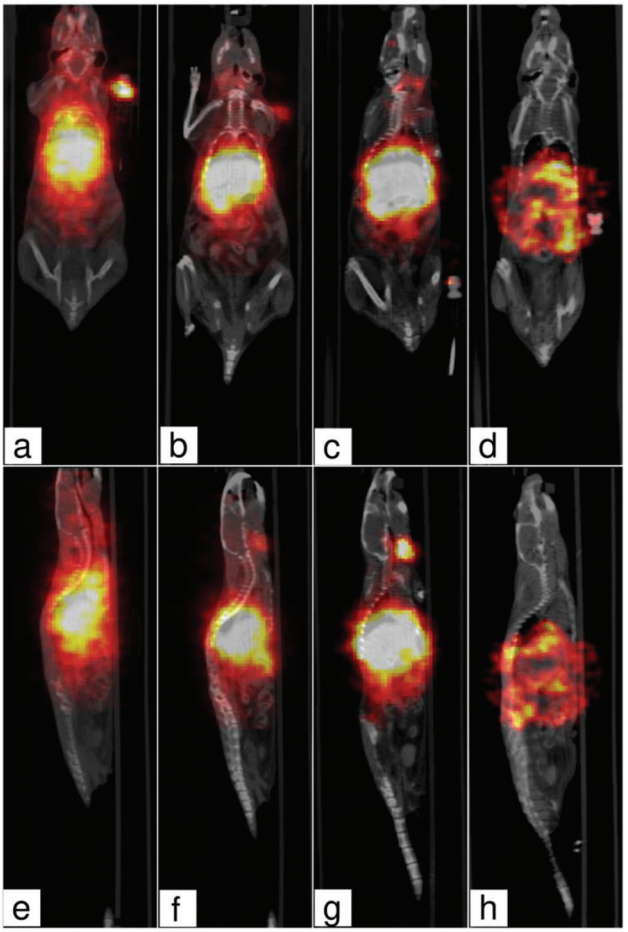

Fig. 5 SPECT/CT images of a mouse after (a and e) 30 min, (b and f) 1.5 h, (c and g) 24 h, and (d and h) 96 h of intravenous injection of the ^{125}I-labeled $NaYF_4:Yb^{3+}/Er^{3+}$@PEG nanoparticles. Two mice were screened with the same result.

(10 days), suggesting that the particles did not aggregate in PBS buffer (Fig. S10 in the ESI†).

In vitro interactions of $NaYF_4:Yb^{3+}/Er^{3+}$@PEG nanoparticles with HF and HeLa cells

The cytotoxicity of $NaYF_4:Yb^{3+}/Er^{3+}$ and $NaYF_4:Yb^{3+}/Er^{3+}$@PEG nanoparticles was determined with primary fibroblasts (HF) and cervical carcinoma HeLa cell lines using AlamarBlue® cell viability assay (Fig. 4). While $NaYF_4:Yb^{3+}/Er^{3+}$ nanoparticles were slightly cytotoxic only at the two highest concentrations (300 and 600 μg ml^{-1}) on primary HF cells, which are more sensitive than carcinoma cell lines, the viability decreased at these concentrations to 51 and 59%, respectively. $NaYF_4:Yb^{3+}/Er^{3+}$@PEG particles did not show significant toxicity at these two highest concentrations. These differences can be influenced by the modification of the particles with PEG. The cytotoxic effects of both $NaYF_4:Yb^{3+}/Er^{3+}$ and $NaYF_4:Yb^{3+}/Er^{3+}$@PEG nanoparticles were minimal on HeLa cells. The two highest concentrations decreased the viability to 76 and 89% for $NaYF_4:Yb^{3+}/Er^{3+}$ and $NaYF_4:Yb^{3+}/Er^{3+}$@PEG particles, respectively.

In vivo biodistribution SPECT/CT study

Two mice were injected intravenously with ^{125}I-labeled $NaYF_4:Yb^{3+}/Er^{3+}$@PEG nanoparticles in PBS. SPECT/CT scans have shown very fast and complete homogeneous liver uptake (Fig. 5). Most of the activity was already located in the liver 30 min after injection. A partial particle degradation led to free radioiodine radioactivity reuptake into the thyroid gland. Nanoparticles were then slowly excreted by the hepatobiliary route with almost complete relocation to the gastrointestinal tract within 4 days after the injection. The fast liver accumulation is especially advantageous for possible use in NIR-photoablative therapeutic techniques of liver tumors, which are (due to very high blood supply) very difficult to be surgically removed.

Conclusions

For the first time, highly colloidally stable biocompatible ^{125}I-labeled $NaYF_4:Yb^{3+}/Er^{3+}$@PEG nanoparticles were successfully developed and used for dual-modal NIR optical and SPECT/CT imaging. This radiolabeling strategy is of general use, allowing toolbox-like design to construct multi-decorated coatings. The

 This journal is © The Royal Society of Chemistry 2017

Open Access Article. Published on 02 October 2017. Downloaded on 8/16/2024 3:05:35 PM.
This article is licensed under a Creative Commons Attribution 3.0 Unported Licence.

particles showed excellent long-term colloidal stability in albumin-containing PBS without any aggregation and/or dissolution. *In vitro* cytotoxicity proved that the $NaYF_4$:Yb^{3+}/Er^{3+}@PEG particles did not show significant toxicity for cancer cells and primary fibroblast cells. Only naked $NaYF_4$:Yb^{3+}/Er^{3+} nanoparticles were slightly toxic at concentrations >0.3 mg ml^{-1}. Moreover, the particles were tested on the non-tumor mice by noninvasive *in vivo* PET/SPECT imaging, showing very fast and complete homogeneous liver uptake.

Bimodal upconversion ^{125}I-labeled $NaYF_4$:Yb^{3+}/Er^{3+}@PEG nanoparticles that simultaneously integrate different imaging modalities and include specific targeting moieties and/or drugs can prospectively facilitate effective monitoring and treatment of early stage diseases and tumors, as well as following photoablative therapy of hard-to-resect liver tumors. Moreover, the nanoparticles can suit noninvasive short- and long-term *in vivo* imaging to track fate of the nanoparticles in the organism and/or can become a superior tool for photodynamic therapy if they contain a suitable photosensitizer.

Conflicts of interest

There are no conflicts of interest to declare.

Acknowledgements

Financial support of the Czech Science Foundation (15-01897S) is gratefully acknowledged. Synthesis of PEG-Ner was supported by grant from the Ministry of Health of the Czech Republic (16-30544A). Biological imaging was supported by the Ministry of Education Youth and Sports of the Czech Republic (LM2015062 Czech-BioImaging and SVV 260371/2017).

References

1 W. Cai and X. Chen, *J. Nucl. Med.*, 2008, **49**, 113S.
2 S. Teipel, A. Drzezga, M. J. Grothe, H. Barthel, G. Chételat, N. Schuff, P. Skudlarski, E. Cavedo, G. B. Frisoni, W. Hoffmann, J. R. Thyrian, C. Fox, S. Minoshima, O. Sabri and A. Fellgiebel, *Lancet Neurol.*, 2015, **14**, 1037.
3 V. Pansare, S. Hejazi, W. Faenza and R. K. Prud'homme, *Chem. Mater.*, 2012, **24**, 812.
4 J. Key and J. F. Leary, *Int. J. Nanomed.*, 2014, **9**, 711.
5 Y. Xing, J. Zhao, P. S. Conti and K. Chen, *Theranostics*, 2014, **4**, 290–306.
6 P. A. Valdés, D. W. Roberts, F. K. Lu and A. Golby, *Neurosurg. Focus*, 2016, **40**, E8.
7 F. Auzel, *Chem. Rev.*, 2004, **104**, 139.
8 M. Haase and H. Schafer, *Angew. Chem., Int. Ed.*, 2011, **50**, 5808.
9 C. Liu, Y. Hou and M. Gao, *Adv. Mater.*, 2014, **26**, 6922.
10 Z. Song, Y. G. Anissimov, J. Zhao, A. V. Nechaev, A. Nadort, D. Jin, T. W. Prow, M. S. Roberts and A. V. Zvyagin, *J. Biomed. Opt.*, 2013, **18**, 061215.
11 M. González-Béjar, L. Francés-Soriano and J. Pérez-Prieto, *Front. Bioeng. Biotechnol.*, 2016, **4**, 47.
12 X. Li, F. Zhang and D. Zhao, *Chem. Soc. Rev.*, 2015, **44**, 1346.
13 B. Zhou, B. Shi, D. Jin and X. Liu, *Nat. Nanotechnol.*, 2015, **10**, 924.
14 U. Kostiv, O. Janoušková, M. Šlouf, N. Kotov, H. Engstová, K. Smolková, P. Ježek and D. Horák, *Nanoscale*, 2015, **7**, 18096.
15 B. R. Smith and S. S. Gambhir, *Chem. Rev.*, 2017, **117**, 901.
16 G. Jalani, R. Naccache, D. H. Rosenzweig, L. Haglund, F. Vetrone and M. Cerruti, *J. Am. Chem. Soc.*, 2016, **138**, 1078.
17 S. K. Maji, S. Sreejith, J. Joseph, M. Lin, T. He, Y. Tong, H. Sun, S. W. Yu and Y. Zhao, *Adv. Mater.*, 2014, **26**, 5633.
18 W. Fan, W. Bu and J. Shi, *Adv. Mater.*, 2016, **28**, 3987.
19 G. Tian, X. Zhang, Z. Gu and Y. Zhao, *Adv. Mater.*, 2015, **27**, 7692.
20 Y. Chen, S. Chatterjee, A. Lisok, I. Minn, M. Pullambhatla, B. Wharram, Y. Wang, J. Jin, Z. M. Bhujwalla, S. Nimmagadda, R. C. Mease and M. G. Pomper, *J. Photochem. Photobiol., B*, 2017, **167**, 111.
21 R. Li, Z. Ji, J. Dong, C. H. Chang, X. Wang, B. Sun, M. Wang, Y. P. Liao, J. I. Zink, A. E. Nel and T. Xia, *ACS Nano*, 2015, **9**, 3293.
22 O. Plohl, M. Kraft, J. Kovač, B. Belec, M. Ponikvar-Svet, C. Würth, D. Lisjak and U. Resch-Genger, *Langmuir*, 2017, **33**, 553.
23 F. Zhang, *Photon Upconversion Nanomaterials*, Springer, 2015.
24 S. M. Tehrani, W. Lin, S. Rosenfeldt, G. Guerin, Y. Lu, Y. Liang, M. Drechsler, S. Förster and M. A. Winnik, *Chem. Mater.*, 2016, **28**, 501.
25 R. Li, Z. Ji, C. H. Chang, D. R. Dunphy, X. Cai, H. Meng, H. Zhang, B. Sun, X. Wang, J. Dong, S. Lin, M. Wang, Y. P. Liao, C. J. Brinker, A. Nel and T. Xia, *ACS Nano*, 2014, **8**, 1771.
26 R. Li, Z. Ji, H. Qin, X. Kang, B. Sun, M. Wang, C. H. Chang, X. Wang, H. Zhang, H. Hzou, A. E. Nel and T. Xia, *ACS Nano*, 2014, **8**, 10280.
27 C. H. Evans, *Biochemistry of the Lanthanides*, Springer, 1990.
28 D. Bekah, D. Cooper, K. Kudinov, C. Hill, J. Seuntjens, S. Bradforth and J. Nadeau, *J. Photochem. Photobiol., A*, 2016, **329**, 26.
29 H. Schafer, P. Ptacek, K. Kompe and M. Haase, *Chem. Mater.*, 2007, **19**, 1396.
30 J. V. Jokerst, T. Lobovkina, R. N. Zare and S. S. Gambhir, *Nanomedicine*, 2011, **6**, 715.
31 P. Cao, L. Tong, Y. Hou, G. Zhao, G. Guerin, M. A. Winnik and M. Nitz, *Langmuir*, 2012, **28**, 12861.
32 J.-C. Boyer, M.-P. Manseau, J. I. Murray and F. C. J. M. van Veggel, *Langmuir*, 2010, **26**, 1157.
33 Y. Que, C. Feng, G. Lu and X. Huang, *ACS Appl. Mater. Interfaces*, 2017, **9**, 14647.

Open Access Article. Published on 02 October 2017. Downloaded on 8/16/2024 3:05:35 PM.
This article is licensed under a Creative Commons Attribution 3.0 Unported Licence.

34 U. Kostiv, I. Kotelnikov, V. Proks, M. Šlouf, J. Kučka, H. Engstová, P. Ježek and D. Horák, *ACS Appl. Mater. Interfaces*, 2016, **8**, 20422.
35 G. R. Kieczykowski, R. B. Jobson, D. G. Melillo, D. F. Reinhold, V. J. Grenda and I. Shinkai, *J. Org. Chem.*, 1995, **60**, 8310.
36 C. Li, T. R. Greenwood, Z. M. Bhujwalla and K. Glunde, *Org. Lett.*, 2006, **8**, 3623.
37 P. Černoch, Z. Černochová, J. Kučka, M. Hrubý, S. Petrova and P. Štěpánek, *Appl. Radiat. Isot.*, 2015, **98**, 7.
38 N. Bogdan, F. Vetrone, G. A. Ozin and J. A. Capobianco, *Nano Lett.*, 2011, **11**, 835.
39 J. W. M. Bolte and N. M. J. Modo, *Design and Application of Nanoparticles in Biomedical Imaging*, Springer, 2017.
40 D. H. Lee and R. A. Condrate, *J. Mater. Sci.*, 1999, **34**, 139.
41 H. Matsuura and T. Riiyazawa, *J. Polym. Sci., Part A: Polym. Chem.*, 1969, **7**, 1735.
42 K. Shameli, M. B. Ahmad, S. D. Jazayeri, S. Sedaghat, P. Shabanzadeh, H. Jahangirian, M. Mahdavi and Y. Abdollahi, *Int. J. Mol. Sci.*, 2013, **13**, 6639.

This journal is © The Royal Society of Chemistry 2017